Draft version October 2, 2025
Typeset using LaTeX **twocolumn** style in AASTeX7

Dust Recycling and Icy Volatile Delivery (DRIVE): A Novel Method of Volatile Enrichment in Cold Giant Planets

Eric R. Van Clepper,[1] Felipe Alarcón,[2] Edwin Bergin,[3] and Fred J. Ciesla[1]

[1]*Department of the Geophysical Sciences, University of Chicago, 5734 S. Ellis Avenue, Chicago, IL 60637, USA*
[2]*Dipartimento di Fisica, Università degli Studi di Milano, Via Celoria 16, 20133 Milano, Italy*
[3]*Department of Astronomy, University of Michigan, 323 West Hall, 1085 S. University Avenue, Ann Arbor, MI 48109, USA*

(Received September 9, 2025; Revised September 15, 2025)

Submitted to ApJL

ABSTRACT

Giant planet atmospheres are thought to reflect the gas phase composition of the disk when and where they formed. However, these atmospheres may also be polluted via solid accretion or ice sublimation in the disk. Here, we propose a novel mechanism for enriching the atmospheres of these giant planets with volatiles via pebble drift, fragmentation, and ice sublimation. We use a combination of 3D hydrodynamic simulations, radiative transfer, and particle tracking to follow the trajectories and resulting temperatures of solids in a disk containing an embedded planet forming outside the CO snowline. We show that small dust can become entrained in the meridional flows created by the giant planet and advected above the disk midplane where temperatures are well above the sublimation temperature of CO. This transport of small grains occurs over 10 kyr timescales, with individual micron-sized grains cycling between the midplane and surface of the disk multiple times throughout the planetary accretion stage. We find that this stirring of dust results in sublimation of CO gas above the snow surface in the dust trap created exterior to the giant planet, leading to super-solar CO abundances in the pressure bump. This mechanism of Dust Recycling and Icy Volatile Enrichment in cold giant planets, which we call the DRIVE effect, may explain compositions of both wide separation exoplanets as well as Jupiter in our own Solar System.

Keywords: Exoplanets (498), Hydrodynamical simulations (767), Planet formation (1241), Protoplanetary disks (1300), Solar system astronomy (1529)

1. INTRODUCTION

A major goal of studying protoplanetary disk (PPD) evolution is to connect observed exoplanets with their formation regions within the disk. A primary method to do so is to compare atmospheric C/O of giant planets with expected gas phase disk compositions of different regions of the disk based on sublimation temperatures of C- and O-bearing molecules (K. I. Öberg et al. 2011). The C/O ratio of the planet atmosphere should reflect the C/O ratio of the disk gas based on the location of the snowlines. Observations of young giant planets and PPDs, however, have revealed an apparent mismatch between disk and planetary compositions. While directly detected giant planets, located at large separations from their host star, tend to have stellar to slightly super-stellar C/O (C.-C. Hsu et al. 2024; E. Nasedkin et al. 2024), disks are inferred to have much higher C/O ratios in these cold regions, with gas-phase C/O exceeding unity (see discussion in, e.g. E. A. Bergin et al. 2024). Additionally, cold giant planets have been observed to have an enriched metallicity compared to their host star, both in our solar system and around other stars (e.g. S. K. Atreya et al. 2020; C. Li et al. 2020; E. Nasedkin et al. 2024; W. O. Balmer et al. 2025; J. D. Lothringer et al. 2025). The gas phase metallicity in the outer disk, however, should be low, with the majority of major C- and O-bearing molecules frozen out onto grains (E. A. Bergin et al. 2024). Thus although the gas in the cold outer regions of PPDs is carbon rich and low metallicity, the atmospheres of giant planets that are inferred to form in these regions of the disk have lower C/O and higher metallicity than their host star. As such, there appears to be disconnect between the composition of the

giant planet atmospheres and the gaseous disks in which they form.

One of the current leading theories for giant planet formation is pebble accretion, wherein planetary cores grow by accreting drifting pebbles through the disk (M. Lambrechts & A. Johansen 2014). In this model, planetary core composition is set by the composition of these solids, both the refractory grain as well as any volatiles that may be present as an ice mantle. Once the core grows large enough, it opens a gap in the disk, halting the inward drift of solids and shutting off pebble accretion (M. Lambrechts et al. 2014). Though the pebble isolation mass depends on the gas scale height and turbulence, typical masses are on the order of a few 10s of Earth Masses (B. Bitsch et al. 2018). At this stage, the core accretes gas from the disk, undergoing a runaway growth phase until the gas disk dissipates (J. B. Pollack et al. 1996). Importantly, the solid ice and gas should have distinct C/O ratios depending on the temperatures of the disk relative to snowlines of major C- and O-bearing molecules, such as H_2O, CO_2, and CO, with the ice typically having a lower C/O compared to the surrounding gas due to the presence of water ice (K. I. Öberg et al. 2011). So while the core of the planet may initially accrete the oxygen rich pebbles, once the planet reaches the pebble isolation mass the atmosphere should largely reflect the relatively carbon-rich composition of the gas where the planet formed.

One way to alter the composition giant planet atmosphere is if the planet grows inside of a snowline in the disk. As pebbles drift from the outer disk, they will pass snowlines, enriching the region interior in volatiles (J. N. Cuzzi & K. J. Zahnle 2004; F. Ciesla & J. Cuzzi 2006; K. I. Öberg & E. A. Bergin 2016; R. A. Booth et al. 2017; C. Danti et al. 2023). If a planet grows just interior to one of these snowlines, then its atmosphere should become enriched in those volatiles (A. D. Schneider & B. Bitsch 2021a,b). Additionally, if the ice present on these grains carries with it trapped noble gasses, this sublimation may explain the enrichment of both volatiles and noble gasses in Jupiter's atmosphere (N. Monga & S. Desch 2014; O. Mousis et al. 2019; S. K. Atreya et al. 2020). This model is particularly attractive as snowlines can also create local pebble pile-ups, which may help to initiate core formation (J. Drążkowska & Y. Alibert 2017; G. Andama et al. 2022; T. C. H. Lau et al. 2022). This, however, requires the planetary core to accrete gas from the region just interior to the snowline, and cannot explain any enrichment of a given species exterior to its respective snowline.

Recent models have shown that the growing planetary embryo, surrounding gas, and smaller solids all interact with one another, complicating the otherwise simple picture of giant planet formation. One such complication is the meridional flow patterns of gas accretion onto the planet in 3D (W. Kley et al. 2001; A. Morbidelli et al. 2014; J. Szulágyi et al. 2014; J. Fung & E. Chiang 2016; R. Teague et al. 2019; E. Lega et al. 2024). Hydrodynamic simulations of gap opening planets in 3D show that gas moves outward, away from the planet along the spiral arms at the midplane. Gas flows are away from the midplane at the gap edges and fall onto the poles of the planet from 1-3 scale heights above the midplane. Such 3D stirring can entrain small dust, increasing the dust scale height near the planet (J. Bi et al. 2021) and even lead to the accretion of small dust onto the planet (J. Szulágyi et al. 2022; N. Maeda et al. 2024; H. J. Petrovic et al. 2024; E. Van Clepper et al. 2025).

In this work, we examine the chemical consequences of the vertical stirring immediately outside a growing planet, and the delivery of volatiles to the planetary atmosphere. First, we describe our methodological approach, including disk hydrodynamic simulations, radiative transfer modeling, Monte-Carlo particle integrations, and dust growth and fragmentation simulations. Using the results of these combined modeling techniques, we show that the Dust Recycling and Icy Volatile Enhancement (DRIVE) effect can lead to an enhancement of the gas phase abundance of CO, even exterior to the CO snowline. We discuss these results in the context of Jupiter and other directly imaged exoplanets and compare with other mechanisms of volatile enhancement in giant planet atmospheres.

2. METHODOLOGY

To explore the consequences of dust stirring near an embedded giant planet, we model the gas disk using single-fluid FARGO3D hydrodynamic simulations (F. Masset 2000; P. Benítez-Llambay & F. S. Masset 2016) with 256 radial cells ranging from 30 au to 337.5 au, 512 cells in azimuth from 0 to 2π, and 32 cells in colatitude spanning from 1.32 rad to the disk midplane. We simulate a 0.05 $M_\odot$ disk around a 1 $M_\odot$ star. We include a 318 $M_\oplus$ giant planet at a fixed separation of 75 au using a mass taper over the first 100 orbits. The disk aspect ratio at the planet separation was set to 0.05. The disk is simulated for 1000 orbits, and the resulting structure is used to determine the dust temperature in post-processing, following F. Alarcón & E. A. Bergin (2024). The resulting gas density and velocity structure are shown in Figure 1, with the velocity shown relative to the planet, $\tilde{v}$, with $\tilde{v}_r < 0$ indicating gas flow towards the planet. Near the midplane, gas is primarily flowing away from the planet along the spiral arms. Gas ac-

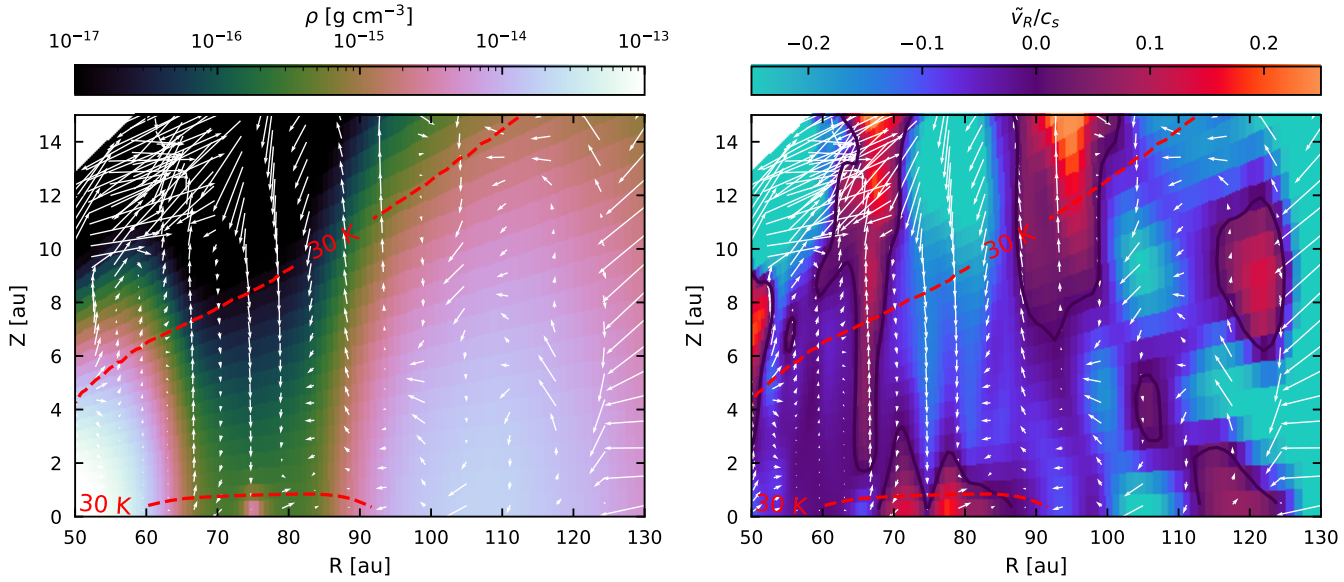

Figure 1. Azimuthally averaged gas density (left) and gas radial velocity relative to the planet (right) for our FARGO3D disk model contatining a Jupiter mass planet at 75 au. The CO sublimation surface at 30 K recovered from our RADMC-3D model is indicated in both panels by the red dashed line. The region near the embedded planet is heated from accretion heating onto the planet, resulting in higher temperatures at the midplane in the gap. Gas advection relative to the local sound speed is also indicated by white arrows. Gas advection is primarily outward along the midplane near the planet, with significant vertical flows away from the midplane at the gap edge and in the pressure bump at 100 au.

cretion tends to be onto the poles of the planet, as is expected from meridional flow patterns (W. Kley et al. 2001; A. Morbidelli et al. 2014; J. Szulágyi et al. 2014). Within the pressure bump near 100 au, gas advection tends to be vertically away from the midplane.

The temperature within the disk is determined using RADMC-3D (C. P. Dullemond et al. 2012) including radiation from the central star, emission from the embedded planet, and viscous heating (see F. Alarcón & E. A. Bergin 2024). For the temperature structure, we assume a constant dust-to-gas mass ratio of 0.01, with the solid mass entirely in small dust. The outer disk is characterized by passive heating, with the upper layers of the disk being hotter than the regions close to the midplane (E. I. Chiang & P. Goldreich 1997). Near the planet, accretion heating raises the local temperature, increasing the dust and gas temperature at the midplane in the gap, as can be seen via the iso-temperature contour in Figure 1.

CO is highly volatile in protoplanetary disks. The temperature at which it begins to appreciably come off the grains depends on the CO binding energy and surface area of grains available. The binding energy of CO is uncertain and depends on the ice mixture on the mantle of the grain, with literature values ranging from 855 K (D. McElroy et al. 2013) up to 1500 K (E. C. Fayolle et al. 2016), suggesting freeze-out temperatures of ∼20 - 30 K. Throughout this work, we use a conservative assumption for the CO sublimation temperature of 30 K, corresponding to a midplane snowline location of 45 au, interior to the planet location of 75 au modeled here. The location of the CO snowline is shown by the red dashed line in Figure 1. While this temperature is an approximation, the results presented here do not depend the exact temperature, and we discuss differing heights of the CO sublimation surface later. Although, heating from the embedded planet increases the midplane temperature above the CO sublimation temperature near the edge of the gap, the main region of the pressure bump that is above 30 K is above $Z/R \approx 0.1$, slightly above 1 scale height at this location of the disk.

Small solids in the disk, which serve as the feedstock of planetesimals and planets, can be grouped via their aerodynamic properties and interactions with the gas. These aerodynamic properties are defined via the Stokes number, St, which is the dimensionless ratio of the stopping time to the orbital period of the solid. Throughout this work, we refer to two main populations of solids, the small dust and larger pebbles (as in, e.g. T. Birnstiel et al. 2012). Small dust ($\mathrm{St} < 10^{-3}$) is defined as those solids which are primarily coupled with the gas, and whose dynamics are strongly affected by gas advection and turbulence. The dynamics of larger pebbles ($10^{-3} < \mathrm{St} \lesssim 1$) are mainly driven via gas drag-induced radial drift (S. J. Weidenschilling 1977). Pebbles also experience significant settling, with typical scale heights

much less than that of the gas, in contrast with the smaller dust which has a comparable scale height to the gas (A. N. Youdin & Y. Lithwick 2007).

Once the physical conditions within the disk are known, we track the location and temperature of pebble and dust tracer particles of constant size using the 3D Monte-Carlo particle tracking technique described in E. Van Clepper et al. (2025). Particles are started at the midplane exterior to the gap opened by the giant planet, here at about 100 au. We examine particle sizes ranging from submicron, St $< 10^{-5}$, up to 1 cm in size, St ≈ 1. Because the solids are integrated using a constant particle size, their Stokes numbers vary throughout the integration, with the Stokes number inversely proportional to the gas density. As a result, particles' Stokes numbers decrease in the pressure bump, where gas densities are at a local maximum, and increase in the gap and away from the midplane, where gas densities are lower. Where Stokes numbers are given here, it is the Stokes number for solids at the midplane at 100 au as a means to compare between the 3D constant size integration and 1D dustpy simulations, described further below. Particles of all sizes are integrated forward in time including random diffusion for 1 Myr, with their locations recorded every 10 years ($\sim$ 0.01 orbital period). At each time, the temperature of the particles are interpolated from the RADMC-3D outputs. While the RADMC-3D simulations only consider the small, well-coupled dust to determine the dust temperature, we assume that all dust and gas are in thermal equilibrium; that is, the temperature of all sizes of dust and the gas is the same at a given location of the disk.

While particles in our simulations remain at fixed sizes, we also use dustpy simulations (S. M. Stammler & T. Birnstiel 2022) to model the dust size evolution for the disk. We match the dustpy surface density to the FARGO3D simulation including a Jupiter mass planet at 75 au. The disk is initialized with a MRN-like dust size distribution (J. S. Mathis et al. 1977) in the outer disk with a dust-to-gas mass ratio of 0.01. As the fragmentation velocity of dust is uncertain, we do two simulations, one with a fragmentation velocity of 1 m/s and one with 10 m/s. Both simulations assume a constant α viscosity parameter of $\alpha = 10^{-3}$ as in our FARGO3D runs. The initial conditions and dust size distribution after 1 Myr of evolution for both simulations are shown in Figure 2. The location of the pressure bump in the dustpy simulations is centered at 101 au, agreeing with the full 3D hydrodynamic simulations.

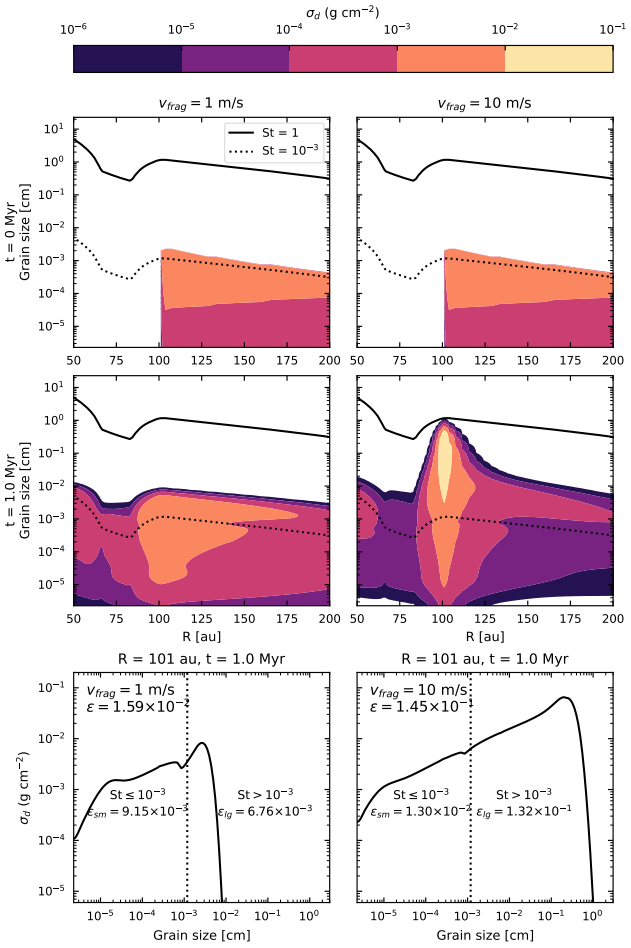

Figure 2. Dust distribution as a function of size and radius from dustpy simulations showing the initial conditions of the dust size distribution (top row) and after 1 Myr of evolution (center row) for a disk containing a Jupiter mass planet located at 75 au. We examine disks with particle fragmentation velocities of 1 m/s (left column) and 10 m/s (right column). The grain size distribution in the pressure bump at 101 au is shown in the bottom row. Regardless of dust fragmentation velocity, we see an enhancement of small dust less than St = 10^{-3} (dotted line) in the pressure bump. The total dust-to-gas mass ratio, ε, is labeled in each plot, where the initial dust-to-gas is $\varepsilon = 0.01$ in the outer disk. The dust-to-gas mass ratios for grain with St $\leq 10^{-3}$, ε_{sm}, and St $> 10^{-3}$, ε_{lg} are also shown. For the case with larger fragmentation velocity, while the total dust mass is higher and grains reach much larger sizes, the total mass of dust with St $\leq 10^{-3}$ is about 0.01 in both cases.

3. THE DRIVE MECHANISM

Combining these techniques, we examine the stirring of small dust in the pressure bump created by a giant planet. We find that a natural consequence of dust growth is the concentration of solids in the dust trap and stirring of small dust to higher and warmer regions

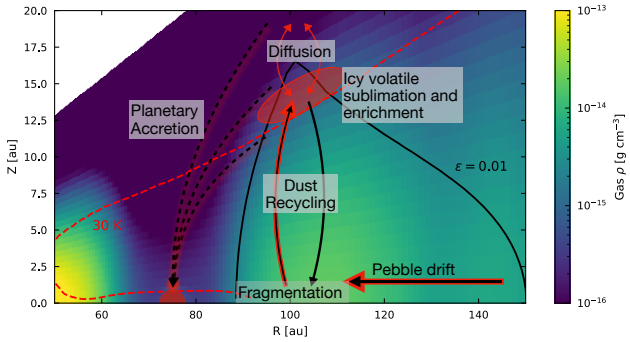

Figure 3. Cartoon schematic of the DRIVE effect enriching the atmosphere of a giant planet with volatiles. Larger pebbles trap volatiles from the outer disk and transport them to the pressure bump created by the giant planet via radial drift. Here, fragmentation creates fine dust, which can be lofted away from the midplane, leading to sublimation of ice mantles on the dust and enriching the gas above the snow surface with volatiles. This volatile rich gas can then be accreted onto the planet, resulting in a volatile enriched atmosphere. The dust, due to the lower gas density at the surface of the disk, decouples from the gas and can settle back to the midplane as a bare grain, fractionating the volatile elements from the more refractory solids. Here, the color shows the azimuthally averaged gas density from our FARGO3D simulations. The solid black contour outlines the region of the disk where total dust-to-gas mass ratio is equal to 0.01 in our dustpy simulations, with higher dust-densities below this contour. The transport of icy pebbles is represented by the black and red solid arrows, while black arrows represent bare grains and red arrows represent CO gas. Meridional flows onto the planet including entrained CO gas are illustrated by the red and black dashed arrows. The approximate location of the CO snowline at 30 K is also included.

of the disk, enriching the gas accreted onto the planet in volatiles. Figure 3 shows a cartoon illustration of this process highlighting the essential ingredients: pebble drift, fragmentation, meridional circulation, and volatile sublimation. We refer to this process as "Dust Recycling and Icy Volatile Enrichment" (DRIVE), whereby small dust grains undergo a cycle of growth and fragmentation, transporting volatile ices above the snow surface and sublimating CO into the gas phase. The gas, now enriched in volatiles sublimated from the grains, can then be accreted onto the planet and incorporated into the giant planet atmosphere. Thus, we do not require giant planets to grow interior of the midplane snowline to inherit volatile gas into their atmosphere. Rather, the planet may form exterior to the snowline and inherit volatile gas that has been sublimated by small grains lofted above the snow surface. This provides a novel way to enrich the atmospheres of cold giant planet after they have reached the pebble isolation mass.

3.1. *Solid concentration and fragmentation*

Once they reach the pebble isolation mass, giant planets create pressure maxima external to their orbit (R. R. Rafikov 2002), where radial drift is halted and solids can concentrate (S. J. Weidenschilling 1977; M. Lambrechts et al. 2014; C. P. Dullemond et al. 2018). In these regions, grains grow to a certain maximum size before relative velocities exceed fragmentation velocities, breaking apart larger pebbles into a cascade of small dust grains (T. Birnstiel et al. 2011, 2012). Indeed, numerical simulations have shown that fragmentation is a common outcome in the pressure bump exterior to a giant planet (J. Drążkowska et al. 2019; S. M. Stammler et al. 2023; L. E. J. Eriksson et al. 2024).

Our dustpy simulations show that regardless of fragmentation velocities assumed, the pressure bump exterior to the planet becomes enriched in both large pebbles and small dust. Because these dust grains in the bump are supplied by inward drift of ice-rich pebbles, the increase in dust mass also corresponds with an increase in total CO in the bump. Figure 2 shows the grain size distribution in the pressure bump, where both the dust-to-gas mass ratio, ε, and maximum grain size reach peak values. We also show the dust-to-gas mass ratios for small and large grains, ε_{sm} and ε_{lg} respectively, where we define small grains as dust (St$\leq 10^{-3}$) and large grains as pebbles (St$> 10^{-3}$). In both the model with low fragmentation velocity and high fragmentation velocity, the total dust-to-gas mass ratio is increased above the initial value of 10^{-2}, with $\varepsilon = 1.59 \times 10^{-2}$ and 1.45×10^{-1} respectively. Despite differences in the total dust-to-gas ratios, the value of ε_{sm} is comparable in both cases, $\varepsilon_{sm} = 0.915 \times 10^{-2}$ and 1.3×10^{-2} for $v_{frag} = 1$ m/s and 10 m/s respectively. Regardless of fragmentation velocity, we see an enhancement not only in the total dust-to-gas mass ratio, but also an enhancement of the small, well-coupled dust with St $\leq 10^{-3}$, approximately equal to the initial value of 0.01 in the pressure bump exterior to the planet. This enhancement in small dust is key to the delivery of CO ice to the gas, as the small dust is more mobile in the pressure bump and can be lofted to regions in the disk above the CO sublimation temperature, sublimating CO from the ice phase into the gas.

3.2. *Dust recycling and ice sublimation*

Next, we examine the thermal histories of solids of different sizes immediately exterior to the planet. The larger pebbles, here ranging from 100 µm to 1 cm, tend to stay near the cold midplane, while grains smaller than 10 µm can be lofted to higher elevations and reach higher temperatures. Figure 4 shows the maximum temper-

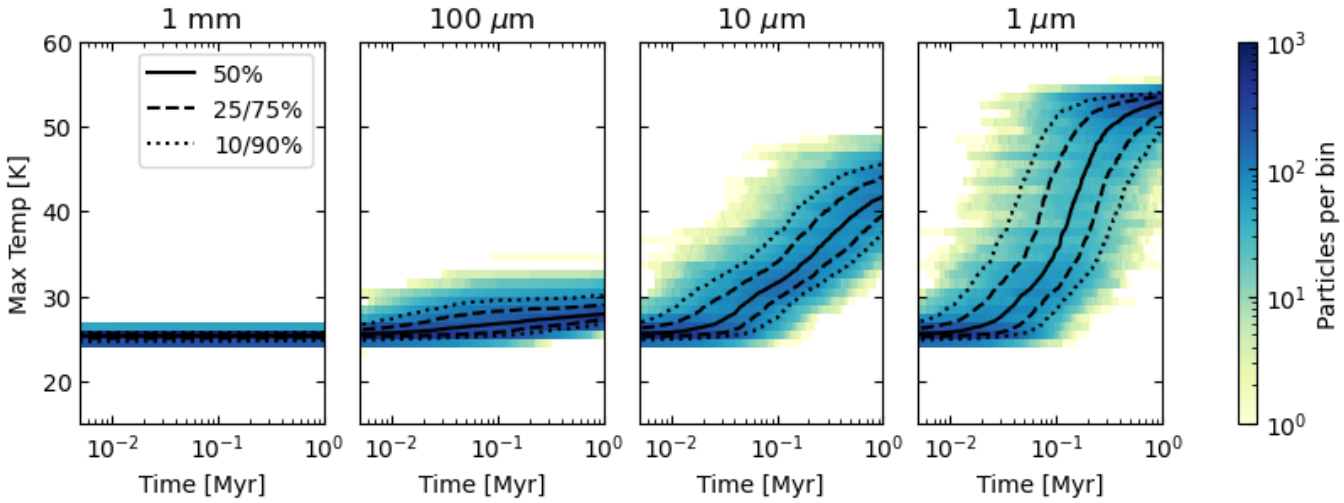

Figure 4. The maximum temperature reached by particles of different sizes, ranging from 1 mm to 1 μm (right column) for particles starting at the midplane at 100 au. The colormap shows the number of particles out of 1000 total that have reached a given temperature as a function of time. Also indicated in each plot by a solid line is the 50$^{\text{th}}$ percentile for maximum temperature reached as a function of time. The dashed lines show the 25$^{\text{th}}$ and 75$^{\text{th}}$ percentiles, and dotted line show 10$^{\text{th}}$ and 90$^{\text{th}}$ percentiles. While large particles are not heated much above the midplane temperature, solids below 10 μm in size (St $\lesssim 10^{-3}$ at the midplane experience heating. All of these dust particles experience temperatures above 30 K by 1 Myr.

ature reached by 1000 particles of different sizes over time. Dust with sizes $\leq$ 10 μm (St $\leq 10^{-3}$) experience temperatures much higher than the midplane temperature of 21 K. After 0.1 Myr, 75% of micron-sized dust has reached temperatures well above the CO sublimation temperature of 30 K with 100% of the small dust reaching temperatures above 30 K by 1 Myr. This trend is similar for 10 μm, while the larger 100 μm show only about 10% of grains reaching above 30 K, with no millimeter or larger grains reaching the CO sublimation temperature. These larger grains tend to experience some heating from the luminous planetary embryo, but here it is insufficient for CO sublimation, and we focus on the heating of small grains at the surface of the disk.

The locations and temperatures over time for one hundred 1 μm sized examples particles are shown in Figure 5. Although these small dust grains tend to experience the highest degree of heating, they spend the majority of the time near the midplane and low temperatures. When these solids are heated, it is typically during brief excursions to upper layers of the disk, before returning to the cold midplane, as has been found in studies of disks not containing a planet (e.g. F. J. Ciesla & S. A. Sandford 2012; J. B. Bergner & F. Ciesla 2021; L. Flores-Rivera et al. 2024).

This migration of small grains to the disk surface is enhanced via the meridional flows created by the planet. 3D hydrodynamic simulations have shown that planet-induced pressure bumps can significantly increase the scale height of small dust (J. Bi et al. 2021; J. Szulágyi et al. 2022). In Figure 5, we also show the trajectory of the particle that experiences the highest degree of heating near the time when it reaches this temperature. The planet creates meridional flow patterns that can entrain small particles, lifting them near the surface of the disk. Here, where the dust grains are heated, they sublimate CO ice to the gas phase, increasing the CO gas abundance above the snow surface. In Figure 5, the highlighted particle's position and temperature is shown over only 20 kyr, yet the dust particle is transported vertically over 2 gas scale heights. While the timescale for vertical transport via turbulence in the disk is $\tau_{turb} = (\alpha\Omega)^{-1} \approx 200$ kyr for $\alpha = 10^{-3}$, dust particles simulated here tend to be transported on much shorter timescales, indicating gas advection as the dominant transport mechanism.

While these grains initially follow the gas advection away from the midplane, they do not tend to be accreted by the planet. This is because as the small grains are lofted, the gas density decreases, resulting in an increase to the particle's Stokes number. Thus, while experiencing heating at the surface of the disk, the grains decouple from the gas flow and settle back to the midplane, where – now depleted in CO ice – they may coagulate into larger pebbles (S. Krijt & F. J. Ciesla 2016; W. Misener et al. 2019). Any gas phase CO that is not accreted onto the planet may diffuse back below the snow surface and freezeout again as ice. Even if some amount of CO vapor returns to the grain, that grain remains in the pressure bump, where fragmentation will resupply the

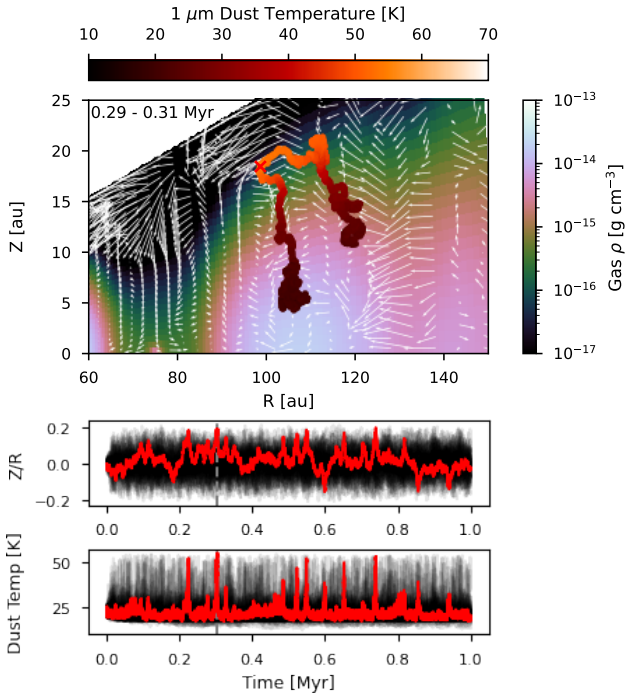

Figure 5. (Top) Particle trajectory of the tracer particle reaching the maximum temperature, with the hottest point labeled with a red dot. The background color and arrows show the azimuthally averaged gas density and advection. This particle is lofted to high altitude following the meridional gas circulation in the disk, reaching temperatures up to 55 K. The particle's temperature along its trajectory is shown by the color of line. The particle temperature is shown over 20 kyr to demonstrate the particle's trajectory before and after reaching the hottest point at 0.3 Myr. This particle's height above the midplane (middle) and temperature (bottom) are also shown as a function of time over the full 1 Myr integrated by the red lines. Examples of other particles are also shown in black, indicating the highlighted particle's trajectory and temperature are typical of other similarly sized particles.

fine dust, which can again transport that CO ice back to the disk surface, repeating the cycle of grain lofting and volatile sublimation. As a result, a single micron sized grain may transport CO ice to the surface of the disk multiple times over the disk lifetime.

3.3. *Giant planet atmosphere enrichment*

We have shown that embedded giant planets are expected to both create dusty pile-ups exterior to their orbit and that dust grains in this pile-up should experience heating when they diffuse to the upper regions of the disk. These small grains are resupplied via the fragmentation of inward drifting, volatile-rich pebbles from the outer disk. As a result, small grains will tend to carry these volatile ices to the surface regions of the disk, where they can be accreted onto the planet, enriching the planetary envelope in volatiles, even in the case where the planet is located outside of the midplane snowline.

To determine the magnitude of enhancement we expect above the snow-surface, we assume a steady-state dust distribution from our dustpy simulations. We assume that this disk structure has evolved from an initially homogeneous disk, with constant dust-to-gas and CO abundance given by ε_0 and $X_{\rm CO,0}$ respectively. Throughout disk evolution, CO entirely freezes onto grain surfaces such that the CO-to-grain mass ratio remains constant. Additionally, we assume that grains heated above 30 K are able to fully sublimate CO from the ice-phase to the gas phase, such that the CO gas abundance, $X_{\rm CO}$, is proportional to the mass of grains heated above 30 K. Finally, we assume that in this steady-state approximation CO is able to diffuse vertically, such that $X_{\rm CO}$ is constant everywhere above the height where $T = 30$ K.

Under these assumptions, the total abundance of CO gas above the snow surface is given by

$$X_{\rm CO} = \frac{\beta(Z_{\rm sub})}{\varepsilon_0} X_{\rm CO,0} = f_{\rm CO} X_{\rm CO,0}, \tag{1}$$

where $\beta(Z_{\rm sub})$ is the integrated dust-to-gas ratio above $Z_{\rm sub}$, where $Z_{\rm sub}$ is the height above the midplane where ice sublimation occurs. The enhancement in CO above the initial abundance is given by $f_{\rm CO} = \beta(Z_{\rm sub})/\epsilon_0$, where $\beta(Z_{\rm sub})$ is given by the equation

$$\beta(Z_{sub}) = \frac{\int_{Z_{\rm sub}}^{\infty} \int_{a_0}^{a_{\rm max}} \eta(a,z)\ {\rm d}a\ {\rm d}z}{\int_{Z_{\rm sub}}^{\infty} \rho(z)\ {\rm d}z}. \tag{2}$$

Here, $\rho(z)$ is the gas density and $\eta(a,z)$ is defined such that $\int_{a_0}^{a_{max}} \eta(a,z)\ {\rm d}a = \rho_{\rm dust}(z)$ gives the total volume density of dust at height z, with a_0 and $a_{\rm max}$ being the smallest and largest grains present. By definition, $\beta(0) = \varepsilon$, and for any degree of grain settling, $\beta(Z > 0) \leq \varepsilon$.

Because dustpy is a 1D simulation, we assume a vertical distribution of dust and grains from the surface density and gas scale height. The gas scale height, $h = c_s\Omega$ (where Ω is the local Keplerian frequency and c_s is the sound speed), is assumed from a E. I. Chiang & P. Goldreich (1997) like midplane temperature profile. The dust scale height, h_a, is written as in (A. N. Youdin & Y. Lithwick 2007)

$$h_a = \sqrt{\frac{\delta}{\delta + {\rm St}_a}} h, \tag{3}$$

where δ is the vertical diffusivity of the dust and ${\rm St}_a$ is the Stokes number of a solid of size a. We define

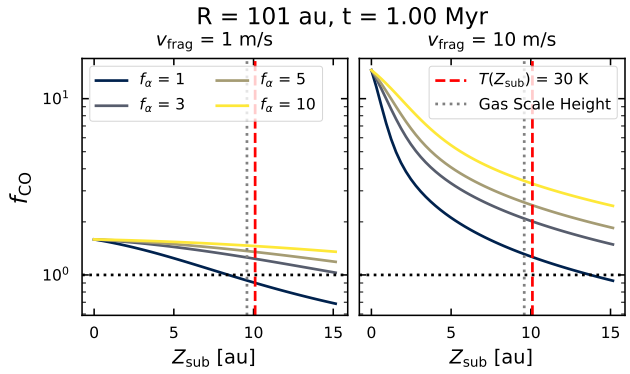

Figure 6. Expected CO abundance relative to the initial abundance, $f_{\rm CO}$, as a function of $Z_{\rm sub}$ and f_α. $f_{\rm CO}$ is calculated from the dustpy simulation after 1 Myr of evolution in the pressure bump for fragmentation velocities of 1 m/s (left) and 10 m/s (right). The CO sublimation surface where dust temperatures reach 30 K is shown by the red dashed line, while the gas scale height is shown by the gray dotted line. The dust scale-height is increased using a diffusivity of $f_\alpha\alpha$, accounting for vertical stirring as a result of meridional flows. We find that for $Z_{\rm sub}/R < 0.1$, dust densities (and thus CO abundances) are near or above expected solar metallicities in all cases, with $X_{\rm CO}$ up to $3X_{\rm CO,0}$ for the best case tested here.

$\delta = f_\alpha\alpha$, where f_α is a dimensionless vertical turbulence parameter, to account for an increase in the vertical scale height of dust as a result of stirring via meridional flows exterior to the planet (J. Bi et al. 2021; J. Szulágyi et al. 2022). While this value of f_α is uncertain, we test a variety of values ranging from $1 \leq f_\alpha \leq 10$.

The enhancement in CO relative to the initial abundance, $f_{\rm CO}$, is plotted as a function of $Z_{\rm sub}$ at R = 101 au, the location of the pressure bump and dust trap for our dustpy simulations, in Figure 6. Here, we see that fragmentation and stirring both tend to increase the mass of dust present above the sublimation surface. We indicate both the gas scale height and the height at which T = 30 K ($Z/R \approx 0.1$). For this sublimation temperature, CO abundances directly exterior to the planet range from slightly sub-solar up to a maximum of 3× solar abundance if $f_\alpha = 10$. While disk turbulence is difficult to constrain, observations of disks containing ring and gap structures have shown that some rings may be "puffier" than others, with vertical turbulence up to $\alpha \approx 10^{-2}$ (K. Doi 2021; M. Villenave et al. 2025), corresponding to $f_\alpha = 10$ in our model. We note that 30 K assumed here is likely an upper limit for the temperature of CO sublimation. If CO begins to sublimate off of the grain at lower temperatures, this will correspond with lower values of $Z_{\rm sub}$ and an increase of $\beta(Z_{\rm sub})$. Thus a lower sublimation temperature – and lower sublimation height in the disk – will increase the expected volatile enrichment onto the planet.

While low fragmentation velocities tend to create more small dust, the concentration of total solids in the pressure bump remains relatively low compared with the higher fragmentation velocity model (See section 3.1). For the high fragmentation velocity case, pebble growth and inward drift concentrates solids in the bump, leading to more fragmentation and a higher density of all grains, including the small dust necessary to transport CO ice above the snow surface. Although the bulk of the mass is contained in large grains near the midplane, the "tail" of the mass distribution towards smaller grains results in significant dust mass above 1 scale height; $\beta(h)/\varepsilon_0 > 1$ even for the case with no additional vertical stirring ($f_\alpha = 1$). The maximum enhancement to dust in the upper disk, and thus enhancement in CO gas, would occur from efficient inward drift of pebbles from the outer disk followed by fragmentation in the bump. We note that fragmentation in the pressure bump exterior to a giant planet is expected to be enhanced, due to increased relative velocities in the spiral arms (J. Drążkowska et al. 2019; L. E. J. Eriksson et al. 2024). Additional vertical stirring as a result of planetary meridional flows, as expected from 3D simulations (J. Bi et al. 2021; J. Szulágyi et al. 2022), will act to further increase the delivery of volatile ice above the CO snow surface.

The ingredients for the DRIVE mechanism are expected to be present regardless of where the planet forms. The detailed implications for the composition of the planet will depend on its formation location relative to the various snow lines that would exist throughout the disk. For example, CO_2 may also sublimate off the lofted grains considered here, but due to its higher binding energy, will only do so for those grains that reach temperatures in excess of ∼50 K. This would lead to a lower enhancement in CO_2 than CO because of the former's higher snow surface. Were the planet forming just outside the midplane CO_2 snow line, however, the planet may receive an enrichment in CO_2, while the CO would be present at roughly solar abundance as its snow line is located much further out in the disk and drifting pebbles would be absent of CO ice. However, it is clear that linking a planetary atmosphere's composition to its formation history cannot be done simply in 1D models, but must consider the 2D evolution of the disk.

Here we highlight the importance of the 3D snow *surface*, rather than focus on the midplane snowline. Previous studies have highlighted the "cold finger" effect, where dust growth and settling can deplete volatiles from the surface layer of the disk, enriching the midplane (R. Meijerink et al. 2009; S. Krijt et al. 2016; E.

Van Clepper et al. 2022). In the presence of a giant planet, however, the dust pile-up will lead to frequent collisions and fragmentation, replenishing the supply of small grains exterior to the planet. These small grains cycle between the midplane and upper regions of the disk on 10 kyr timescales (less than the diffusive mixing time), carrying their volatile ice mantle with them. Here, grains sublimate their volatiles into the gas phase, creating a volatile rich gas environment above the snow surface. Given the giant planet accretes gas from above one scale height (R. Teague et al. 2019; A. J. Cridland et al. 2020), this volatile rich gas will be readily accreted into the atmosphere of the giant planet. A. J. Cridland et al. (2020) showed that the vertical accretion of icy pebbles from above one scale height in a chemically static disk can lower the atmospheric C/O of giant planets by incorporating O-rich molecules present in the gas phase in the warm upper regions of the disk. Here, we show that inward drift and fragmentation of pebbles and increases the dust-to-gas ratio well above 0.01. With the dust mass exceeding expected solar values above the CO sublimation surface, so too should the CO abundance exceed solar abundance. Thus we expect the C/H and O/H of the disk gas to be enhanced, increasing C/H and O/H of the planetary atmosphere.

3.4. *Caveats to the model*

The magnitude of the volatile delivery onto the planet will depend in detail on the production of fine dust from pebbles and the heating of that dust, which itself depends on the interplay between grain growth, fragmentation, transport, and heating in 3D. Modeling these processes together, however, is a computationally expensive task and will depend on many factors, including the disk mass, viscosity, accretion rate, and pebble flux. Here, we examine some of the assumptions and limitations of the modeling work presented here.

First, we examine our dust population assumptions from the 1D dustpy model presented in Section 3.1. In 2D, for example, when small solids are lofted they will collide with other small solids, resulting in growth via sweep-up. S. Krijt & F. J. Ciesla (2016) studied dust growth and settling in a 1D vertical slice of an axisymmetric disk in the absence of a planet. They showed that even for high dust-to-gas ratios up to 0.1, as would be expected in the pressure bump exterior to the planet, small dust grains can still reach heights up to the gas scale height before growing and settling back to the midplane. W. Misener et al. (2019) expanded this to a 2D disk ($R-Z$) including growth, fragmentation, settling, and drift, and showed similar results, with small grains typically reaching 1-2 gas scale heights in the disk shortly after a collision before growing and settling again. Here, though, we again emphasize the role of the meridional flows, which will serve to further increase the dust scale height, as shown here and in other work (J. Bi et al. 2021; J. Szulágyi et al. 2022). Thus, we expect even in the case of dust-sweep up at altitude, small grains should be able to deliver volatiles to the warm atmosphere of the disk.

Next, we consider how this effect might operate at other snowlines throughout the disk. For grains to be heated as they are lofted in the disk, this requires the gas temperature to be lower at the midplane and higher at the surface of the disk. While this is true for disks where heating is primarily a result of irradiation, viscous heating at the midplane can also provide a source of heat. Viscous heating depends on the mass accretion rate and disk mass (N. Calvet et al. 1994), and as a result is more dominant in the inner disk where midplane densities are highest. As such, DRIVE should be most apparent in the outer disk, where the surface of the disk is hotter than the midplane. "Cold" snow surfaces, such as the CO and CO_2 sublimation fronts, are thus most likely to undergo this process of grain lofting and sublimation, while "hotter" snowlines, like the H_2O snowline or "soot line" (location of refractory carbon sublimation, M. E. Kress et al. 2010; J.-E. Lee et al. 2010; J. Li et al. 2021), are more likely to have colder disk surfaces, and thus may not be as susceptible to thermal desorption at the surface of the disk. Enhanced UV radiation at the surface of the disk, however, may drive grain chemistry including desorption in these regions (N. F. W. Ligterink et al. 2024).

Finally, as dust grains are the primary transport mechanism for volatiles in the DRIVE model, grain surface chemistry will play an important role setting the gas-phase volatile abundances. Irradiation, for example, may dissociate CO into atomic C and O, resulting in the production of secondary ice species with different binding energies (see, e.g., J. B. Bergner & F. Ciesla 2021; N. F. W. Ligterink et al. 2024; A. J. Cridland et al. 2025). If the resulting primary C- and O-bearing have drastically different binding energies from one another (or from CO) then this may effect the resulting metallicity and C/O of volatiles sublimated from the grains and ultimately the planetary atmosphere. This will, however, depend on the relative timescales involved between grain surface and gas phase chemistry and optical depth of the dust, and should be studied in more detail using dynamic chemical models.

4. COMPARISON WITH OTHER MECHANISMS

We present the DRIVE mechanism as an additional means by which giant planet atmospheres may become enriched in volatile species. While the different mechanisms of giant planet atmosphere enrichment are not mutually exclusive from one another, each may be dominant in different disk conditions and leave distinct traces of that formation pathway on the formed planet. In this section, we briefly summarize some such models and differences with our model presented here.

4.1. *Pebble drift across snowlines*

The process here is similar to the enrichment of volatiles at snowlines as a result of pebble drift (K. I. Öberg & E. A. Bergin 2016; R. A. Booth et al. 2017; K. Zhang et al. 2020), although these models require the planet form interior to the snowline, while the DRIVE model presented here allows for planet to incorporate these volatile even when forming outside of the midplane snowline. Enrichment via pebble drift across snowlines requires large pebbles to drift past midplane snowlines, enhancing the abundance of a given volatile species. Here, we enhance the gas-phase with volatile species via the vertical lofting of small grains above the snow surface. Additionally, the pebble drift model of enhancement would predict that CO should be enhanced in the inner disk as CO-rich pebbles drift across the CO snowline. Disk observations, however, have shown that CO is depleted rather than enhanced interior to the CO snowline (K. Zhang et al. 2019).

4.2. *Planetesimal Accretion*

Another way to enhance the metallicity of the atmosphere of giant planets is via accretion and ablation of planetesimals. If these planetesimals originate in the outer disk, then they may be volatile rich (S. K. Atreya et al. 1999). Jupiter, for example, may have formed in the outer disk, beyond the N_2 snowline, accreting C, N, and O from icy planetesimals (A. D. Bosman et al. 2019; K. I. Öberg & R. Wordsworth 2019), before migrating to its current day location. This inward migration may further act to shepherd planetesimals onto the planet, enriching the envelope of closer in exoplanets (S. Shibata et al. 2020, 2022) and Jupiter (S. Shibata & R. Helled 2022) if it migrated in from the outer disk. This assumes there are ample planetesimals in the disk to be accreted, however dynamical models show scattering, rather than accretion, may dominate interactions between planets and planetesimals (L. E. J. Eriksson et al. 2022).

An important aspect of the DRIVE model is the separation of volatiles from their refractory carriers, resulting in preferential accretion of volatiles over solid dust grains. This refractory-to-volatile ratio in the atmospheres of planets is expected to differ depending on the mechanism of enrichment (J. D. Lothringer 2021). Thus this refractory-to-volatile ratio may help to differentiate between planetesimal accretion, pebble accretion, and the DRIVE mechanism . The DRIVE model presented here provides a novel way to transport volatile carbon and oxygen from the outer disk into the atmosphere of an accreting giant planet, providing a new mechanism to set the C/O and metallicity of giant planet atmospheres separate distinct from planetesimal accretion models.

4.3. *Heating from the planetary embryo*

We emphasize that DRIVE does not require solids to filter through the gap, nor pass within the envelope of the embedded planet. Previous studies have shown that pressure traps may be "leaky" and small particles may filter from the outer disk to the inner disk (C. P. Dullemond et al. 2018; P. Weber et al. 2018; T. Haugbølle et al. 2019; S. M. Stammler et al. 2023; E. M. Price et al. 2025; E. Van Clepper et al. 2025). In doing so, they may pass by the luminous, embedded planet (H. J. Petrovic et al. 2024), heating those grains and sublimating ice back to the disk (M. N. Barnett & F. J. Ciesla 2022; H. Jiang et al. 2023; Y. Wang et al. 2023; A. J. Cridland et al. 2025). Additionally, in 3D, accreted grains tend to pass near the planet following the gas accretion flow, which transports grains near the surface of the disk (J. Szulágyi et al. 2022; H. J. Petrovic et al. 2024; E. Van Clepper et al. 2025). As a result, even when grains are accreted onto the planet, some amount of thermal processing, including sublimation of the ice mantle, is likely to occur during this accretion phase. In the DRIVE mechanism presented here, solids are heated by irradiation from the host star at the atmosphere of the disk rather than from the planet itself, and thus is not dependent on the amount of solid mass that may pass the growing the planet. In this way, the DRIVE mechanism does not depend on the "leakiness" of the gap, and is expected to function in either strong or weak pressure bumps.

5. CONCLUSION

In this work, we present a novel method to enrich the atmospheres of cold giant planets with volatiles. This "Dust Recycling and Icy Volatile Enrichment" (DRIVE) effect relies on the following disk processes to occur:

1. Dust and pebbles are concentrated at the local pressure maxima exterior to the gap carved by a giant planet due to inward drift of icy pebbles from the outer disk.

2. Small dust is created via pebble fragmentation, which is transported upwards through diffusion and advection via the meridional flows created by the planet and exposed to higher temperatures at the surface of the disk, resulting in the sublimation of volatiles into the gas phase.

3. The giant planet accretes gas from above one scale height in the disk, which has been enriched in volatiles sublimated from the small dust.

All of these are expected via the current understanding of giant planet formation, and combined will enrich giant planet atmospheres with volatiles, even after the planet has reached the pebble isolation mass and outside the midplane snowline. Similar to how radial drift can enrich volatile abundances interior to midplane snowlines, we expect that this combined fragmentation and lofting should increase volatile abundances above the snow surface as well. While some of the sublimated volatiles may diffuse downward and re-freeze onto grain surfaces, these grains will continue to cycle back to the upper region of the disk, sublimating volatiles again. This concentration of dust in the pressure bump may lead to enhancements of up to 3× Solar abundance of CO above the snow surface.

Under the DRIVE mechanism, we expect wide separation giant planets to become enriched in volatile C and O, increasing measured metallicity in their atmospheres. This effect may explain the observed mismatch between gas-phase composition of disks and atmospheric composition of cold giant planets, which are currently difficult to explain using either pebble or planetesimal accretion models (E. A. Bergin et al. 2024; E. Nasedkin et al. 2024; W. O. Balmer et al. 2025). Additionally, DRIVE provides a novel way to separate volatile ice from refractory carriers. Thus, bulk metallicity measurements of exoplanets inferred from single molecular abundances may not reflect this partitioning, and refractory-to-volatile ratios may be key in understanding giant planet formation history (J. D. Lothringer 2021; J. D. Lothringer et al. 2025). Jupiter's enhanced metallicity, for example, is largely based on the enhancement of volatile species, including noble gasses, carbon, nitrogen, and oxygen (see, S. K. Atreya et al. 2020, and references therein). Understanding the relative composition of refractory elements will be key to understanding Jupiter's bulk metallicity and differentiating possible origin scenarios.

While we have explored the dust growth and fragmentation, disk hydrodynamics, radiative transfer, and particle dynamics separately here, there are important feedback mechanisms that may affect the magnitude of the DRIVE effect. The chemistry of the disk is sensitive to the small dust, which is the primary carrier of volatiles, which may act to further alter the C/O and metallicity of the gas near the growing planet. This dust, however, is intricately linked to the gas dynamics, which is in turn driven by interactions with the embedded planet. This small dust also serves as the primary source of opacity in the disk, feeding back on the thermal structure and UV driven chemistry in the disk. Better understanding the evolution of dust in a disk containing an embedded planet will provide many future avenues of research with implications for the chemistry and dynamics of disks and the planets that form within.

ACKNOWLEDGMENTS

This work was completed in part with resources provided by the University of Chicago's Research Computing Center. EVC acknowledges support from NASA FINESST grant 80NSSC23K1380. FA is funded by the European Union (ERC, UNVEIL, 101076613). Views and opinions expressed are however those of the author(s) only and do not necessarily reflect those of the European Union or the European Research Council. Neither the European Union nor the granting authority can be held responsible for them. FJC and EAB acknowledge support from NASA's Emerging Worlds Program, grant 80NSSC20K0333, and NASA's Exoplanets Research Program, 80NSSC20K0259. This material is also based upon work supported by the National Aeronautics and Space Administration under agreement No. 80NSSC21K0593 for the program "Alien Earths." The results reported herein benefited from collaborations and/or information exchange within NASA's Nexus for Exoplanet System Science (NExSS) research coordination network sponsored by NASA's Science Mission Directorate.

Software: `dustpy` (S. M. Stammler & T. Birnstiel 2022), `FARGO3D` (P. Benítez-Llambay & F. S. Masset 2016; F. Masset 2000), `matplotlib` (J. D. Hunter 2007), `numpy` (C. R. Harris et al. 2020). `radmc3d-2.0` (C. P. Dullemond et al. 2012).

REFERENCES

Alarcón, F., & Bergin, E. A. 2024, The Astrophysical Journal, 967, 144, doi: 10.3847/1538-4357/ad3d57

Andama, G., Ndugu, N., Anguma, S. K., & Jurua, E. 2022, Monthly Notices of the Royal Astronomical Society, 512, 5278, doi: 10.1093/mnras/stac772

Atreya, S. K., Hofstadter, M. H., In, J. H., et al. 2020, Space Science Reviews, 216, 18, doi: 10.1007/s11214-020-0640-8

Atreya, S. K., Wong, M. H., Owen, T. C., et al. 1999, Planet. Space Sci., 47, 1243, doi: 10.1016/S0032-0633(99)00047-1

Balmer, W. O., Kammerer, J., Pueyo, L., et al. 2025, The Astronomical Journal, 169, 209, doi: 10.3847/1538-3881/adb1c6

Barnett, M. N., & Ciesla, F. J. 2022, The Astrophysical Journal, 925, 141, doi: 10.3847/1538-4357/ac4417

Benítez-Llambay, P., & Masset, F. S. 2016, The Astrophysical Journal Supplement Series, 223, 11, doi: 10.3847/0067-0049/223/1/11

Bergin, E. A., Booth, R. A., Colmenares, M. J., & Ilee, J. D. 2024, The Astrophysical Journal Letters, 969, L21, doi: 10.3847/2041-8213/ad5839

Bergner, J. B., & Ciesla, F. 2021, The Astrophysical Journal, 919, 45, doi: 10.3847/1538-4357/ac0fd7

Bi, J., Lin, M.-K., & Dong, R. 2021, The Astrophysical Journal, 912, 107, doi: 10.3847/1538-4357/abef6b

Birnstiel, T., Klahr, H., & Ercolano, B. 2012, Astronomy & Astrophysics, 539, A148, doi: 10.1051/0004-6361/201118136

Birnstiel, T., Ormel, C. W., & Dullemond, C. P. 2011, Astronomy & Astrophysics, 525, A11, doi: 10.1051/0004-6361/201015228

Bitsch, B., Morbidelli, A., Johansen, A., et al. 2018, Astronomy & Astrophysics, 612, A30, doi: 10.1051/0004-6361/201731931

Booth, R. A., Clarke, C. J., Madhusudhan, N., & Ilee, J. D. 2017, Monthly Notices of the Royal Astronomical Society, 469, 3994, doi: 10.1093/mnras/stx1103

Bosman, A. D., Cridland, A. J., & Miguel, Y. 2019, Astronomy & Astrophysics, 632, L11, doi: 10.1051/0004-6361/201936827

Calvet, N., Hartmann, L., Kenyon, S. J., & Whitney, B. A. 1994, ApJ, 434, 330, doi: 10.1086/174731

Chiang, E. I., & Goldreich, P. 1997, The Astrophysical Journal, 490, 368, doi: 10.1086/304869

Ciesla, F., & Cuzzi, J. 2006, Icarus, 181, 178, doi: 10.1016/j.icarus.2005.11.009

Ciesla, F. J., & Sandford, S. A. 2012, Science, 336, 452, doi: 10.1126/science.1217291

Cridland, A. J., Bosman, A. D., & Van Dishoeck, E. F. 2020, Astronomy & Astrophysics, 635, A68, doi: 10.1051/0004-6361/201936858

Cridland, A. J., Lega, E., & Benisty, M. 2025, Astronomy & Astrophysics, 693, A86, doi: 10.1051/0004-6361/202451140

Cuzzi, J. N., & Zahnle, K. J. 2004, The Astrophysical Journal, 614, 490, doi: 10.1086/423611

Danti, C., Bitsch, B., & Mah, J. 2023, A&A, 679, L7, doi: 10.1051/0004-6361/202347501

Doi, K. 2021, The Astrophysical Journal

Drążkowska, J., & Alibert, Y. 2017, Astronomy & Astrophysics, 608, A92, doi: 10.1051/0004-6361/201731491

Drążkowska, J., Li, S., Birnstiel, T., Stammler, S. M., & Li, H. 2019, The Astrophysical Journal, 885, 91, doi: 10.3847/1538-4357/ab46b7

Dullemond, C. P., Juhasz, A., Pohl, A., et al. 2012, https://ascl.net/1202.015

Dullemond, C. P., Birnstiel, T., Huang, J., et al. 2018, The Astrophysical Journal Letters, 869, L46, doi: 10.3847/2041-8213/aaf742

Eriksson, L. E. J., Ronnet, T., Johansen, A., et al. 2022, Astronomy & Astrophysics, 661, A73, doi: 10.1051/0004-6361/202142391

Eriksson, L. E. J., Yang, C.-C., & Armitage, P. J. 2024, Monthly Notices of the Royal Astronomical Society: Letters, slae110, doi: 10.1093/mnrasl/slae110

Fayolle, E. C., Balfe, J., Loomis, R., et al. 2016, The Astrophysical Journal Letters, 816, L28, doi: 10.3847/2041-8205/816/2/L28

Flores-Rivera, L., Lambrechts, M., Gavino, S., et al. 2024, arXiv, doi: 10.48550/arXiv.2412.01698

Fung, J., & Chiang, E. 2016, The Astrophysical Journal, 832, 105, doi: 10.3847/0004-637X/832/2/105

Harris, C. R., Millman, K. J., Walt, S. J. v. d., et al. 2020, Nature, 585, 357, doi: 10.1038/s41586-020-2649-2

Haugbølle, T., Weber, P., Wielandt, D. P., et al. 2019, The Astronomical Journal, 158, 55, doi: 10.3847/1538-3881/ab1591

Hsu, C.-C., Wang, J. J., Blake, G. A., et al. 2024, The Astrophysical Journal Letters, 977, L47, doi: 10.3847/2041-8213/ad95e8

Hunter, J. D. 2007, Computing in Science & Engineering, 9, 90, doi: 10.1109/MCSE.2007.55

Jiang, H., Wang, Y., Ormel, C. W., Krijt, S., & Dong, R. 2023, Astronomy & Astrophysics, 678, A33, doi: 10.1051/0004-6361/202346637

Kley, W., D'Angelo, G., & Henning, T. 2001, ApJ, 547, 457, doi: 10.1086/318345

Kress, M. E., Tielens, A. G. G. M., & Frenklach, M. 2010, Advances in Space Research, 46, 44, doi: 10.1016/j.asr.2010.02.004

Krijt, S., & Ciesla, F. J. 2016, The Astrophysical Journal, 822, 111, doi: 10.3847/0004-637X/822/2/111

Krijt, S., Ciesla, F. J., & Bergin, E. A. 2016, The Astrophysical Journal, 833, 285, doi: 10.3847/1538-4357/833/2/285

Lambrechts, M., & Johansen, A. 2014, Astronomy & Astrophysics, 572, A107, doi: 10.1051/0004-6361/201424343

Lambrechts, M., Johansen, A., & Morbidelli, A. 2014, Astronomy & Astrophysics, 572, A35, doi: 10.1051/0004-6361/201423814

Lau, T. C. H., Drążkowska, J., Stammler, S. M., Birnstiel, T., & Dullemond, C. P. 2022, Astronomy & Astrophysics, 668, A170, doi: 10.1051/0004-6361/202244864

Lee, J.-E., Bergin, E. A., & Nomura, H. 2010, ApJL, 710, L21, doi: 10.1088/2041-8205/710/1/L21

Lega, E., Benisty, M., Cridland, A., et al. 2024, Astronomy & Astrophysics, 690, A183, doi: 10.1051/0004-6361/202450899

Li, C., Ingersoll, A., Bolton, S., et al. 2020, Nature Astronomy, 4, 609, doi: 10.1038/s41550-020-1009-3

Li, J., Bergin, E. A., Blake, G. A., Ciesla, F. J., & Hirschmann, M. M. 2021, Science Advances, 7, eabd3632, doi: 10.1126/sciadv.abd3632

Ligterink, N. F. W., Pinilla, P., Van Der Marel, N., et al. 2024, Nature Astronomy, doi: 10.1038/s41550-024-02334-4

Lothringer, J. D. 2021, The Astrophysical Journal

Lothringer, J. D., Bennett, K. A., Sing, D. K., et al. 2025, doi: 10.3847/1538-3881/adc117

Maeda, N., Ohtsuki, K., Suetsugu, R., et al. 2024, The Astrophysical Journal, 968, 62, doi: 10.3847/1538-4357/ad4035

Masset, F. 2000, Astronomy and Astrophysics Supplement Series, 141, 165, doi: 10.1051/aas:2000116

Mathis, J. S., Rumpl, W., & Nordsieck, K. H. 1977, ApJ, 217, 425, doi: 10.1086/155591

McElroy, D., Walsh, C., Markwick, A. J., et al. 2013, Astronomy & Astrophysics, 550, A36, doi: 10.1051/0004-6361/201220465

Meijerink, R., Pontoppidan, K. M., Blake, G. A., Poelman, D. R., & Dullemond, C. P. 2009, The Astrophysical Journal, 704, 1471, doi: 10.1088/0004-637X/704/2/1471

Misener, W., Krijt, S., & Ciesla, F. J. 2019, The Astrophysical Journal, 885, 118, doi: 10.3847/1538-4357/ab4a13

Monga, N., & Desch, S. 2014, The Astrophysical Journal, 798, 9, doi: 10.1088/0004-637X/798/1/9

Morbidelli, A., Szulágyi, J., Crida, A., et al. 2014, Icarus, 232, 266, doi: 10.1016/j.icarus.2014.01.010

Mousis, O., Ronnet, T., & Lunine, J. I. 2019, The Astrophysical Journal, 875, 9, doi: 10.3847/1538-4357/ab0a72

Nasedkin, E., Mollière, P., Lacour, S., et al. 2024, Astronomy & Astrophysics, 687, A298, doi: 10.1051/0004-6361/202449328

Petrovic, H. J., Booth, R. A., & Clarke, C. J. 2024, arXiv. http://arxiv.org/abs/2409.16245

Pollack, J. B., Hubickyj, O., Bodenheimer, P., et al. 1996, Icarus, 124, 62, doi: 10.1006/icar.1996.0190

Price, E. M., Van Clepper, E., & Ciesla, F. J. 2025, ApJ, 979, 37, doi: 10.3847/1538-4357/ad9f35

Rafikov, R. R. 2002, The Astrophysical Journal, 572, 566, doi: 10.1086/340228

Schneider, A. D., & Bitsch, B. 2021a, Astronomy & Astrophysics, 654, A71, doi: 10.1051/0004-6361/202039640

Schneider, A. D., & Bitsch, B. 2021b, Astronomy & Astrophysics, 654, A72, doi: 10.1051/0004-6361/202141096

Shibata, S., & Helled, R. 2022, The Astrophysical Journal Letters, 926, L37, doi: 10.3847/2041-8213/ac54b1

Shibata, S., Helled, R., & Ikoma, M. 2020, Astronomy & Astrophysics, 633, A33, doi: 10.1051/0004-6361/201936700

Shibata, S., Helled, R., & Ikoma, M. 2022, Astronomy & Astrophysics, 659, A28, doi: 10.1051/0004-6361/202142180

Stammler, S. M., & Birnstiel, T. 2022, The Astrophysical Journal, 935, 35, doi: 10.3847/1538-4357/ac7d58

Stammler, S. M., Lichtenberg, T., Drążkowska, J., & Birnstiel, T. 2023, Astronomy & Astrophysics, 670, L5, doi: 10.1051/0004-6361/202245512

Szulágyi, J., Binkert, F., & Surville, C. 2022, The Astrophysical Journal, 924, 1, doi: 10.3847/1538-4357/ac32d1

Szulágyi, J., Morbidelli, A., Crida, A., & Masset, F. 2014, The Astrophysical Journal, 782, 65, doi: 10.1088/0004-637X/782/2/65

Teague, R., Bae, J., & Bergin, E. A. 2019, Nature, 574, 378, doi: 10.1038/s41586-019-1642-0

Van Clepper, E., Bergner, J. B., Bosman, A. D., Bergin, E., & Ciesla, F. J. 2022, The Astrophysical Journal, 927, 206, doi: 10.3847/1538-4357/ac511b

Van Clepper, E., Price, E., & Ciesla, F. J. 2025, The Astrophysical Journal, 980, 201, doi: 10.3847/1538-4357/ada8a4

Villenave, M., Rosotti, G. P., Lambrechts, M., et al. 2025, A&A, 697, A64, doi: 10.1051/0004-6361/202553822

Wang, Y., Ormel, C. W., Huang, P., & Kuiper, R. 2023, MNRAS, 523, 6186, doi: 10.1093/mnras/stad1753

Weber, P., Benítez-Llambay, P., Gressel, O., Krapp, L., & Pessah, M. E. 2018, The Astrophysical Journal, 854, 153, doi: 10.3847/1538-4357/aaab63

Weidenschilling, S. J. 1977, Monthly Notices of the Royal Astronomical Society, 180, 57, doi: 10.1093/mnras/180.2.57

Youdin, A. N., & Lithwick, Y. 2007, Icarus, 192, 588, doi: 10.1016/j.icarus.2007.07.012

Zhang, K., Bergin, E. A., Schwarz, K., Krijt, S., & Ciesla, F. 2019, The Astrophysical Journal, 883, 98, doi: 10.3847/1538-4357/ab38b9

Zhang, K., Bosman, A. D., & Bergin, E. A. 2020, The Astrophysical Journal Letters, 891, L16, doi: 10.3847/2041-8213/ab77ca

Öberg, K. I., & Bergin, E. A. 2016, The Astrophysical Journal Letters, 831, L19, doi: 10.3847/2041-8205/831/2/L19

Öberg, K. I., Murray-Clay, R., & Bergin, E. A. 2011, The Astrophysical Journal, 743, L16, doi: 10.1088/2041-8205/743/1/L16

Öberg, K. I., & Wordsworth, R. 2019, The Astronomical Journal, 158, 194, doi: 10.3847/1538-3881/ab46a8